A Continuation Method Applied to the Study of Thermocapillary Instabilities in Liquid Bridges

Jian-Kang Zhang · Bo Xun · Paul G. Chen

Abstract A continuation method is applied to investigate the linear stability of the steady, axisymmetric thermocapillary flows in liquid bridges. The method is based upon an appropriate extended system of perturbation equations depending on the nature of transition of the basic flow. The dependence of the critical Reynolds number and corresponding azimuthal wavenumber on serval parameters is presented for both cylindrical and non-cylindrical liquid bridges.

Keywords Thermocapillary instability ·
Liquid bridge · Continuation method ·
Microgravity

Introduction

Thermocapillary flows refer to motion driven by surface-tension gradients along the free surface. Liquid bridge held between two solid, planar endwalls across which a temperature difference is applied provides a paradigm for the study of such flows owing to its relevance to the float-zone crystal-growth technique.

J.-K. Zhang
School of Aeronautical Science and Engineering,
Beihang University, Beijing 100191, China

B. Xun
National Microgravity Laboratory, Institute of Mechanics,
Chinese Academy of Sciences, Beijing 100190, China

P. G. Chen (✉)
Laboratoire M2P2, UMR 6181, CNRS/Universités
d'Aix-Marseille et Centrale Marseille, 38 rue Frédéric
Joliot-Curie, 13451 Marseille Cedex 20, France
e-mail: chen@L3M.univ-mrs.fr

Considerable attention has been paid to determine the stability boundaries of thermocapillary convection in both cylindrical and non-cylindrical liquid bridges (Wanschura et al. 1995; Nienhüser and Kuhlmann 2002; Shevtsova 2005).

In this paper, instead of conducting time-dependent simulation and directly computing the eigenvalues that characterize a regular (stationary) or a Hopf (oscillatory) bifurcation, we used a continuation method combined with finite-difference method to predict the stability boundaries of the axisymmetric basic state in liquid bridges for a wide range of parameters. The essence of continuation method is to extend the system of equations under investigation by adding an additional parameter and an additional equation so that the combined system is non-singular at limit points where the equations alone are singular (see for example, Henry and Bergeon 2000).

The present paper is an extension of the previous work by Chen et al. (1997) to the case of non-cylindrical liquid bridges where the free-surface shape is determined by the volume of liquid and static pressure difference. For cylindrical liquid bridges we report an updated stability diagram including large-Prandtl-number liquid bridges. For non-cylindrical liquid bridges, a special effort is devoted to show the effect of the relative volume of liquid on the stability of thermocapillary flows.

Problem Formulation

We consider the flow of an incompressible Newtonian fluid confined to a liquid bridge of length L held by surface tension forces between two parallel, coaxial

Fig. 1 Schematic of the
model system
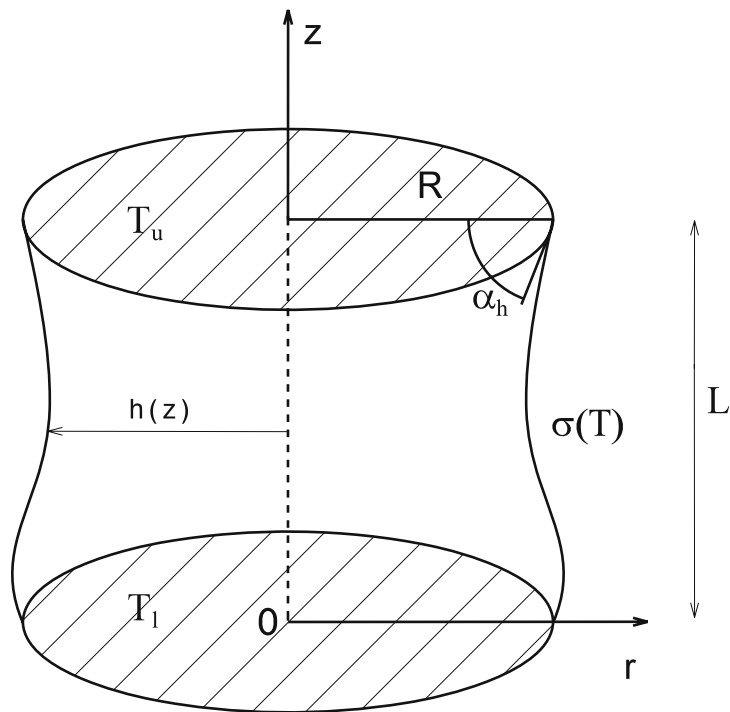
solid rods of equal radii R ($> L/2\pi$). A temperature
difference is imposed over the liquid bridge by pre-
scribing T_u and T_l at the upper and lower disks re-
spectively (see Fig. 1). The liquid is a Newtonian fluid
with constant values of the viscosity μ, the reference
density ρ_0, the specific heat c_p, the thermal conductivity
κ, and the volume expansion coefficient β; $\alpha = \kappa/\rho_0 c_p$
is the thermal diffusivity, and $\nu = \mu/\rho_0$ is the kinematic
viscosity. The surface tension on the free surface is
considered to be a linearly depend on the temperature

$$\sigma = \sigma_0 - \gamma (T - T_0), \tag{1}$$

where σ_0 is the mean surface tension at the reference
temperature $T_0 = \frac{1}{2}(T_l + T_u)$. For common liquids, we
have $\gamma = -\frac{d\sigma}{dT} > 0$, so that there is surface flow from
the hot end toward the cold end. Since the bulk fluids
are viscous, they are dragged along; bulk-fluid motion
results from free surface temperature gradients. The
liquid volume ($= V$) is bounded by a lateral-free sur-
face $r = h(z)$, where z is the vertical coordinate. In the
limit of large mean surface tension, this free-surface
shape is independent of the flow and temperature fields
(see Nienhüser and Kuhlmann 2002).

We consider the fully three-dimensional system in
the usual cylindrical coordinate (r, ϕ, z) with origin
in the center of the bottom end face. Gravity acts
downward along the z-axis. The length (r, z), veloc-
ity vector $\vec{u} = u\vec{e}_r + v\vec{e}_\phi + w\vec{e}_z$, pressure p, tempera-
ture difference $T - T_0$, and time t are referred to

scales R, $\gamma \Delta T/\mu$, $\gamma \Delta T/R$, $\Delta T = T_u - T_l$ and R^2/ν,
respectively. As a result, there arise the following di-
mensionless groups:

$$Re = \frac{\gamma \Delta T R}{\mu \nu}, \ Pr = \frac{\nu}{\alpha}, \ Gr = \frac{g\beta \Delta T R^3}{\nu^2}$$

$$\Gamma = \frac{L}{R}, \ Bi = \frac{\hbar R}{\kappa}, \ Bo = \frac{\rho_0 g L^2}{\sigma_0},$$

Here Re is the surface-tension Reynolds number, Pr
the Prandtl number, Gr the Grashof number, Γ the
aspect ratio, Bi the surface Biot number in which $\hbar$
is the heat transfer coefficient and Bo the static Bond
number. The Marangoni number is $Ma = RePr$. The
relative volume of liquid is $\mathcal{V} = V/\pi R^2 L$. Positive val-
ues of Re and Gr represent the system which is heated
from above, while negative ones correspond to the
system heated from below.

The governing equations for the flow and tempera-
ture fields in the liquid bridge are the Navier–Stokes,
the continuity and the energy equations, subject to the
Boussinesq approximation:

$$\frac{\partial \vec{u}}{\partial t} + Re \, \vec{u} \cdot \nabla \vec{u} = -\nabla p + \nabla^2 \vec{u} + \frac{Gr}{Re}\theta\vec{e}_z, \tag{2}$$

$$\nabla \cdot \vec{u} = 0, \tag{3}$$

$$Pr\left(\frac{\partial \theta}{\partial t} + Re \, \vec{u} \cdot \nabla \theta\right) = \nabla^2 \theta. \tag{4}$$

The boundary conditions at the rigid walls of constant temperature are

$$\vec{u} = 0, \theta = \mp\frac{1}{2}, \text{at } z = 0, \Gamma \tag{5}$$

At the free surface, $r = h(z)$, the kinematic boundary, tangential-stress and heat transfer between liquid zone and surrounding gas are:

$$\vec{n} \cdot \vec{u} = 0, \tag{6}$$

$$\vec{t}_z \cdot (\vec{S} \cdot \vec{n}) = -\vec{t}_z \cdot \nabla\theta, \tag{7}$$

$$\vec{t}_\phi \cdot (\vec{S} \cdot \vec{n}) = -\vec{t}_\phi \cdot \nabla\theta, \tag{8}$$

$$\vec{n} \cdot \nabla\theta = -Bi(\theta - \theta_a(z)). \tag{9}$$

where $\vec{S} = \nabla\vec{u} + (\nabla\vec{u})^T$ is the viscous stress tensor in non-dimensional form. $\theta_a(z)$ is the dimensionless ambient temperature. The vector $\vec{n}$ denotes the outward-directed normal vector of the free surface $h(z)$, and the vectors $\vec{t}_z$ and $\vec{t}_\phi$ denote the unite vectors tangent to the free surface in the (r, z)- and (r, ϕ)-plane, respectively (see Nienhüser and Kuhlmann 2002).

In the limit of large mean surface tension σ_0, the free-surface shape is independent of the flow and temperature fields. Thence at prescribed static Bond number Bo, liquid bridge aspect ration Γ and liquid volume $\mathcal{V}$ (or equivalently a contact angle), the static free-surface shape $h(z)$ can be obtained from the Young-Laplace equation:

$$\frac{h''}{(1+h'^2)^{3/2}} - \frac{1}{h(1+h'^2)^{1/2}} + P_s - Bo\, z = 0, \tag{10}$$

where $h' = dh/dz$. This second-order ordinary equation for $h(z)$ and the constant P_s which is the dimensionless static pressure jump is solved with following three boundary conditions:

$$h(z=0) = h(z=\Gamma) = 1, \tag{11}$$

$$\mathcal{V} = \frac{1}{\Gamma}\int_0^\Gamma h^2(z)dz, \tag{12}$$

or, equivalently,

$$h'(z=\Gamma) = -\tan(\alpha_h - \pi/2). \tag{13}$$

Here α_h is the hot-wall contact angle measured from the rigid disk to the free surface.

Basic Flow

For small Reynolds number the flow in the liquid bridge is steady and axisymmetric ($\partial_t = \partial_\phi = v = 0$) which can

be characterized as a single toroidal vortex in the (r,z)-plane. The system of equations for the basic state, denoted by $\vec{X}(r, z) = (U, 0, W, P, \Theta)$, is obtained from Eqs. 2–9. For the sake of brevity, the details of this system of equations are not given here, it suffices to note that we used finite-difference method in the body-fitted coordinates (ξ, η)

$$\xi = \frac{r}{h}, \ \eta = z \tag{14}$$

which transform the original (curved) physical domain (r,z) onto a rectangular domain (ξ, η). Readers are refereed to Shevtsova (2005) for the details of the transformed equations in the curvilinear coordinates (ξ, η).

The transformed system of equations and boundary conditions are discretized by second-order finite differences on a non-uniform mesh consisting of $N_r \times N_z$ points. The resulting nonlinear difference equations can be written, in the vector form,

$$\boldsymbol{f}(\vec{X}; \lambda, \vec{\mu}) = 0, \tag{15}$$

in which λ is a specific parameter (Re in the present case) and $\vec{\mu}$ is the vector of the remaining parameters of the problem (Pr, Gr, Bi, Γ, Bo and $\mathcal{V}$ or α_h). These parameters are introduced for simplifying the notation in the analysis below. The nonlinear equations (15) are solved by successive Newton–Raphson iteration:

$$\boldsymbol{f}_{\vec{X}}(\vec{X}^n; \lambda, \vec{\mu})d\vec{X}^n = -\boldsymbol{f}(\vec{X}^n; \lambda, \vec{\mu}), \tag{16}$$

$$\vec{X}^{n+1} = \vec{X}^n + d\vec{X}^n. \tag{17}$$

where $\boldsymbol{f}_{\vec{X}} = \partial\boldsymbol{f}/\partial\vec{X}$ is the Jacobian matrix. These iterations continue until the largest variation (relative) of any U, W, P and Θ is less than some convergence tolerance which we set to 10^{-6}. Depending on the parameters of the problem, 4 to 8 iterations can be required provided that initial guess is close enough to the solution. For an appropriate ordering of the grid points and unknowns, the Jacobian matrix $\boldsymbol{f}_{\vec{X}}$ has banded structure with band width, say N_b, being approximatively equal to $\min(8N_r, 8N_z)$. The required band LU factorization and triangular solvers at each Newton–Raphson iteration in (16) are performed by using the DGBFA/DGBSL sequence in the LINPACK subroutine library.

Linear Stability Analysis

The linear stability of the basic state $\vec{X}$ is examined by considering small three-dimensional perturbations, denoted by $\vec{x'} = \{\vec{u'}(r, \phi, z, t), p'(r, \phi, z), \theta'(r, \phi, z)\}$, which

satisfies the linearized perturbation equations (see Chen et al. 1997; Nienhüser and Kuhlmann 2002). Since the basic state is axisymmetric, we can expand the perturbed velocity, pressure and temperature fields in the form

$$
\begin{bmatrix} \vec{u}' \\ p' \\ \theta' \end{bmatrix} = \sum_{m=-\infty}^{+\infty} \begin{bmatrix} \vec{u}^{(m)}(r, z) \\ p^{(m)}(r, z) \\ \theta^{(m)}(r, z) \end{bmatrix} e^{\sigma^{(m)}t + jm\phi},
\tag{18}
$$

where $j = \sqrt{-1}$, m is the (integer) azimuthal wave number, and $\sigma^{(m)}(= \sigma_r + j\omega)$ is the complex growth rate of the corresponding mode perturbation.

Let $\vec{x} = (u, jv, w, p, \theta)^T$ denote a vector of length of $4N + M$, then, the discrete form of the linearized equations can be written as a generalized matrix eigenvalue problem of the form

$$
\boldsymbol{g}(\vec{x}, \vec{X}, Re, m, \vec{\mu}) \equiv A\vec{x} = \sigma B\vec{x},
\tag{19}
$$

where $A \equiv \boldsymbol{g}_{\vec{x}}$ is a real-valued, non-symmetric matrix, and B is a real-valued, diagonal matrix. The Jacobian matrix $\boldsymbol{g}_{\vec{x}}$ is not the same as for the stationary solution $\boldsymbol{f}_{\vec{X}}$ except for the case of $m = 0$, i.e. two-dimensional perturbations. In such case we make no difference between two Jacobian matrices and either of them can be used in the analysis.

The condition that $\max(\sigma_r) = 0$ defines a neutral curve $Re(m)$. The minimum of $Re(m)$ over all m gives a critical value of Re, Re_c and corresponding values of m and ω, m_c and ω_c.

Extended Systems for Locating Bifurcation Points

The general procedure we adopt for locating bifurcation points of the basic state is to solve the equations simultaneously with the conditions satisfied at the bifurcation point. We describe below two appropriate extended systems to locate, respectively, regular (stationary) bifurcations and Hopf (oscillatory) bifurcations. The resulting nonlinear algebraic set of equations are solved by Newton's method to give both the solution at the bifurcation point and the value of the bifurcation parameter.

In order to have a good initial guess for the leading eigenvalues and corresponding eigenvectors of the problem (19), we use the Arnoldi-based scheme which yields iterative approximations to several eigenpairs simultaneously, rather than once a time as in the usual power or inverse iteration methods.

Stationary Bifurcation Points

The system of equations we use to calculate a stationary bifurcation point is the one proposed by Moore and Spence (1980) for locating limit points:

$$
\boldsymbol{f}(\vec{X}, \lambda, \vec{\mu}) = 0,
\tag{20}
$$

$$
\boldsymbol{g}(\vec{x}, \vec{X}, \lambda, m, \vec{\mu}) = 0,
\tag{21}
$$

$$
(\vec{e}_k)^T \cdot \vec{x} = 1,
\tag{22}
$$

where the last equation defines a normalization condition of the eigenvector $\vec{x}$ (note that $\vec{x} \in \vec{R}$), $\vec{e}_k$ is the unit vector with components $(\vec{e}_k)_i = \delta_{ik}$. We solve for the basic state $\vec{X}$, for the bifurcating eigenvector $\vec{x}$ and for the critical value of one specific parameter λ (Re in the present case), at the prescribed values of all the other parameters m and $\vec{\mu}$.

The system of Eqs. 20–22 can be solved by the quadratically convergent Newton iterations

$$
\begin{pmatrix} \boldsymbol{f}_{\vec{X}} & 0 & \boldsymbol{f}_\lambda \\ \boldsymbol{g}_{\vec{X}} & \boldsymbol{g}_{\vec{x}} & \boldsymbol{g}_\lambda \\ 0 & \vec{e}_k^T & 0 \end{pmatrix} \begin{pmatrix} d\vec{X}^n \\ d\vec{x}^n \\ d\lambda^n \end{pmatrix} = - \begin{pmatrix} \boldsymbol{f} \\ \boldsymbol{g} \\ 0 \end{pmatrix},
\tag{23}
$$

starting from a suitable initial guess, until the desired convergence is satisfied. An efficient numerical procedure for (23) is to first solve $\vec{\alpha}_0$ and $\vec{\beta}_0$ from

$$
\boldsymbol{f}_{\vec{X}} \vec{\alpha}_0 = -\boldsymbol{f}; \quad \boldsymbol{f}_{\vec{X}} \vec{\beta}_0 = -\boldsymbol{f}_\lambda,
\tag{24}
$$

then we obtain a set of equations as follows

$$
\begin{pmatrix} \boldsymbol{g}_{\vec{x}} & \boldsymbol{g}_\lambda + \boldsymbol{g}_{\vec{X}} \vec{\beta}_0 \\ \vec{e}_k^T & 0 \end{pmatrix} \begin{pmatrix} d\vec{x}^n \\ d\lambda^n \end{pmatrix} = - \begin{pmatrix} \boldsymbol{g} + \boldsymbol{g}_{\vec{X}} \vec{\alpha}_0 \\ 0 \end{pmatrix},
\tag{25}
$$

Like the procedure (24), we solve $\vec{\alpha}_1$ and $\vec{\beta}_1$ from

$$
\boldsymbol{g}_{\vec{x}} \vec{\alpha}_1 = -(\boldsymbol{g} + \boldsymbol{g}_{\vec{X}} \vec{\alpha}_0); \quad \boldsymbol{g}_{\vec{x}} \vec{\beta}_1 = -(\boldsymbol{g}_\lambda + \boldsymbol{g}_{\vec{X}} \vec{\beta}_0),
\tag{26}
$$

Finally, the required solution updates are easily obtained from

$$
d\lambda^n = -(\vec{e}_k)^T \cdot \vec{\alpha}_1 / (\vec{e}_k)^T \cdot \vec{\beta}_1;
\tag{27}
$$

$$
d\vec{X}^n = \vec{\alpha}_0 + \vec{\beta}_0 d\lambda^n; d\vec{x}^n = \vec{\alpha}_1 + \vec{\beta}_1 d\lambda^n.
\tag{28}
$$

Hopf Bifurcation Points

The prediction of Hopf bifurcations is more complicated than stationary bifurcations as described above. At the Hopf bifurcation point a complex-conjugate pair of eigenvalues with non-zero imaginary parts, $\pm j\omega$,

crosses the imaginary axis. That bifurcation is the solution of the following extended system (Griewank and Reddien 1983) of equations:

$$\boldsymbol{f}(\vec{X}, \lambda, \vec{\mu}) = 0, \tag{29}$$

$$\boldsymbol{g}(\vec{x}, \vec{X}, \lambda, m, \vec{\mu}) = j\omega B\vec{x}, \tag{30}$$

$$(\vec{e}_k + j\vec{e}_k)^T \cdot \vec{x} = j, \tag{31}$$

where the last equation in the set is a normalization condition for the eigenvector $\vec{x}$ (note that $\vec{x} \in \vec{C}$). We solve for the basic state $\vec{X}$, for the bifurcating eigenvector $\vec{x}$, for the angular frequency ω and the critical value of the bifurcation parameter λ, i.e. Re, at the fixed values of all the other parameters m and $\vec{\mu}$.

The system of Eqs. 29–31 is solved by Newton–Raphson iterations from a good enough initial guess. The solution procedure is similar to that described in Section Stationary Bifurcation Points.

Results and Discussion

We present our numerical results both for cylindrical liquid bridges ($\mathcal{V} = 1$, $Bo = Gr = 0$) and non-cylindrical liquid bridges ($\mathcal{V} \neq 1$, $Bo = Gr = 0$) in the case of an adiabatic free surface ($Bi = 0$). Attention is focused on the parametric dependence of the critical Reynolds number Re_c upon such as the Prandtl number Pr, the aspect ratio Γ and the relative liquid-bridge-volume $\mathcal{V}$.

Cylindrical Liquid Bridge

The principal results of the calculations of stability diagram of the thermocapillary flows in a cylindrical liquid bridge for $\Gamma = 1$, are plotted in Fig. 2. A steady, axisymmetric (2D) thermocapillary convection loses its stability to a steady asymmetric (3D) flow when $Pr < 0.06$, the most unstable mode has azimuthal wavenumber $m = 2$. When Pr goes to zero, the critical Reynolds number Re_c remains finite and tends to be a constant indicating the instability is hydrodynamic in origin that breaks the azimuthal symmetry of the basic state. The critical Reynolds number Re_c is strongly dependent on the aspect ratio Γ, we obtained the following relationship for small Pr

$$Re_c = 2160\Gamma^{-5/4}. \tag{32}$$

When $Pr \geq 0.1$, the instability of the basic state is oscillatory with Hopf frequency ω. Two different critical modes were found: $m = 2$ for $Pr \geq 0.9$ and $m = 3$ for $0.1 \leq Pr \leq 0.9$. The Hopf frequency ω has the same dependence on the Prandtl number as critical Reynolds
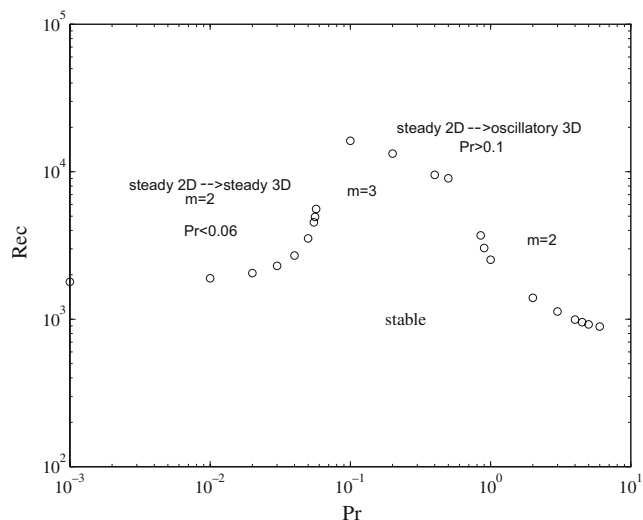
Fig. 2 Stability diagram of the thermocapillary flows in a cylindrical liquid bridge for $\Gamma = 1$, $Bi = 0$ and $Gr = 0$

number, i.e., it decreases with increasing Prandtl number. Previous studies have shown that the large-Prandtl-number instability is due to the surface hydrothermal wave traveling azimuthally, and that there is non axial component of this hydrothermal wave because of the presence of endwalls. The phase speed c of the critical disturbances can be obtained from the computed ω in such a way: $c = \omega/m$. The dependence of c as function of Pr is presented in Fig. 3, showing two different slopes when the most unstable mode changes from $m = 3$ to $m = 2$, but the dependence of c on Pr is less
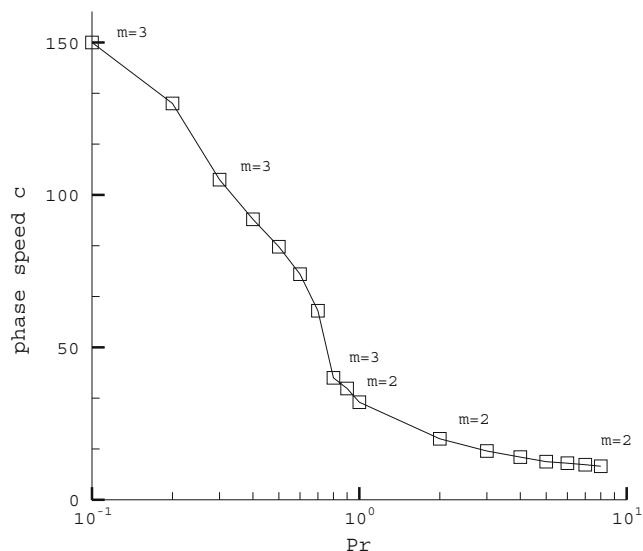
Fig. 3 Phase speed c ($= \omega/m$) of the disturbances at bifurcation point as function of Prandtl number Pr in a cylindrical liquid bridge for $\Gamma = 1$, $Bi = 0$ and $Gr = 0$

pronounced than the dependence of ω on Pr since the correction by m.

In the range of intermediate Pr ($0.06 < Pr < 0.1$), the basic flow exhibits a striking stability property. This feature is due to a competition between two different underlying instability mechanisms and a change of the most unstable mode (see also Levenstam et al. 2001).

More recently, Xun et al. (2008) performed the calculations of stability in the case of large Prandtl numbers ($4 \leq Pr \leq 50$). They found that for liquid bridge with unit aspect ratio the stability boundary exhibits different behaviors in different ranges of large Prandtl numbers: an unexpected increase of Re_c around $8 < Pr < 22$ accompanied with a change of critical azimuthal wavenumber at $m \approx 22$. From the computed surface temperature gradient at bifurcation point, they concluded that the dependence of Re_c on Pr over this Pr range is due to the development of thermal boundary layers at endwalls of liquid bridge, and that the behavior Re_c and m relies more on the *effective* part of liquid bridge beyond the boundary layers. However, it should be pointed out that the critical Marangoni ($Ma_c = Re_c Pr$) increases monotonously with increasing Prandtl number but with different slopes for different m. In this sense, Marangoni number would be more appropriate dimensionless parameter than Reynolds number to characterize the onset of oscillatory thermo-capillary flows for fluids with large Pr.

Non-Cylindrical Liquid Bridge

The validity of the calculated Re_c in the case of non-cylindrical liquid bridge was first confirmed by comparison with the Benchmark (Shevtsova 2005): for example Test case 3.4 ($Pr = 0.01$, $Gr = 0$, $\Gamma = 1.2$ and $\alpha_h = 60$), we obtained $Re_c = 1857$, compared with Benchmark of 1863; the deviation being less than 0.5%.

We present here only the numerical results for a small Pr liquid ($Pr = 0.01$). Attention is paid to determine the influence of the free-surface shape on the critical Reynolds numbers by varying the relative liquid-bridge-volume. As in cylindrical liquid bridge, the first instability of the basic flow, in the range of relative liquid-bridge-volume $\mathcal{V}$ investigated, i.e., $0.6 \leq \mathcal{V} \leq 1.4$, is stationary. The neutral Reynolds number $Re_c(m)$ as function of $\mathcal{V}$ is presented in Table 1. Listed are also the contact angles α_h computed from Eq. 13. It can be seen that the most unstable mode is $m_c = 2$ for moderately concave surface shapes ($\mathcal{V} < 1$) as well as for convex surface shapes ($\mathcal{V} > 1$). The critical wavenumber becomes $m_c = 1$ for slender liquid bridges ($\mathcal{V} < 0.7$). A plausible explanation for the decrease in the critical azimuthal wavenumber is through an

Table 1 Neutral Reynolds numbers $Re_c(m)$ as function of the volume fraction $\mathcal{V}$ for $Pr = 0.01$

$\mathcal{V}$	$Re_c(m)$	m	α_h	$\mathcal{V}$	$Re_c(m)$	m	α_h
0.6	2783	1	30	1.1	2080	2	106
	3412	2					
0.7	2475	1	42	1.2	2371	2	121
	2404	2					
0.8	2008	2	57	1.3	2731	2	134
0.9	1868	2	73	1.4	3131	2	145
1	1900	2	106				

The contact angles α_h (in deg.) are computed from Eq. 13. The parameters are $\Gamma = 1$, $Bo = 0$ and $Gr = 0$

increase in the *effective* aspect ratio Γ'. Indeed, the relationship between the the aspect ratio Γ and the critical azimuthal wavenumber m_c holds for cylindrical liquid bridges (Chen et al. 1997):

$$1.6 \leq m_c \Gamma \leq 3.2.$$

If we substitute Γ by Γ' and relate Γ' with $\mathcal{V}$ in a reasonably way such that:

$$\Gamma' = \Gamma/\sqrt{\mathcal{V}},$$

then the product of the critical azimuthal wavenumber m_c with *effective* aspect ratio Γ', $m_c\Gamma'$, satisfies still the aforementioned relationship for non-cylindrical bridges.

The influence of the relative volume on the critical Reynolds numbers Re_c and corresponding azimuthal wavenumber m_c is plotted in Fig. 4. The crit-
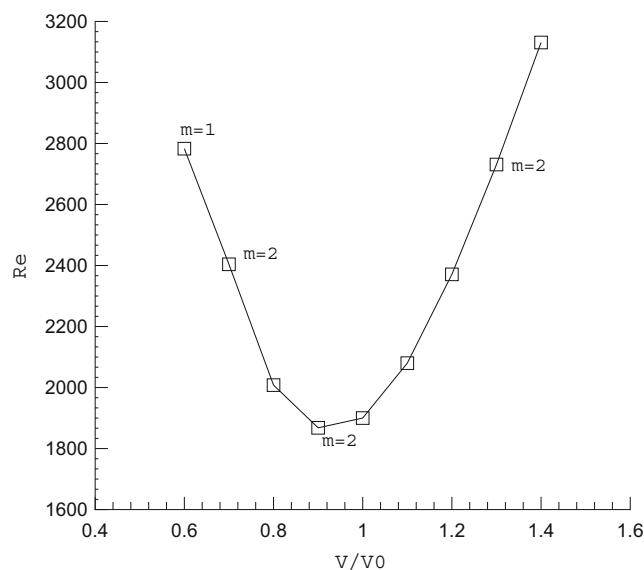
Fig. 4 Dependence of the critical Reynolds numbers Re_c and corresponding azimuthal wavenumber m for $Pr = 0.01$ on the volume fractions $\mathcal{V}$ for non-cylindrical liquid bridges. $\Gamma = 1$, $Bi = 0$ and $Gr = 0$

ical Reynolds numbers are found to take larger values whatever the free-surface shape becomes more concave or more convex. A minimum of $Re_c(\mathcal{V})$ is found for a slightly concave free-surface shape ($\mathcal{V} \approx 0.9$) with a contact angle ($\alpha \approx 70°$), this indicates that a straight cylindrical liquid bridge is not the most stable configuration in terms of hydrodynamic stability property.

Conclusions

We have presented a continuation method combined with finite-difference method to investigate the linear stability of the two-dimensional steady flow in thermocapillary liquid bridges with static free-surface shape. The key idea was to solve an appropriate extended system of perturbation equations, depending on the nature of bifurcation of the basic state. The critical Reynolds numbers and corresponding azimuthal wavenumbers were obtained for a wide range of parameters.

Two distinct instabilities of the two-dimensional flows exists both in cylindrical and non-cylindrical liquid bridges. For small Prandtl numbers the instability is stationary, whereas it is oscillatory for large Prandtl numbers with non-zero Hopf frequency. The latter takes the form of a pair of hydrothermal waves traveling azimuthally. The phase speed of these waves decreases when the Prandtl number is increased.

At a small Prandtl number ($Pr = 0.01$), we found a decrease in the critical azimuthal mode when the liquid bridge becomes more slender. This behavior was interpreted as an increase in the *effective* aspect ratio which was proposed to be scaled with the inverse of the root of the relative volume. The critical Reynolds number takes a smooth minimum near a volume $\mathcal{V} \approx 0.9$.

The present numerical method is robust, particularly for small-Prandtl-number liquid bridges, and computationally very efficient. The code can be run on a usual PC with typical CPU time of a few minutes, depending on numerical resolution. It offers the perspective of further parametric study of the stability problem of thermal convection in liquid bridges with relative high resolution.

References

Chen, G., Lizée, A., Roux, B.: Bifurcation analysis of the thermocapillary convection in cylindrical liquid bridges. J. Cryst. Growth **180**, 638–647 (1997)

Griewank, A., Reddien, G.: The calculation of Hopf points by a direct method. IMA J. Numer. Anal. **3**, 295–303 (1983)

Henry, D., Bergeon, A. (eds.): Continuation Methods in Fluid Dynamics. Notes on Numerical Fluid Mechanics, vol. 74. Vieweg, Wiesbaden (2000)

Levenstam, M., Amberg, G., Winkler, C.: Instabilites of thermocapillary convection in a half-zone at intermediate Prandtl numbers. Phys. Fluids **13**, 807–816 (2001)

Moore, G., Spence, A.: The calculation of turning points of nonlinear equations. SIAM J. Numer. Anal. **17**, 567–576 (1980)

Nienhüser, CH., Kuhlmann, H.C.: Stability of thermocapillary flows in non-cylindrical liquid bridges. J. Fluid Mech. **468**, 35–73 (2002)

Shevtsova, V.: Thermal convection in liquid bridges with curved free surfaces: benchmark of numerical solutions. J. Cryst. Growth **280**, 632–651 (2005)

Xun, B., Chen, P.G., Li, K., Yin, Z., Hu, W.R.: A linear stability analysis of large-Prandtl-number thermocapillary liquid bridges. Adv. Space Res. **41**, 2094–2100 (2008)

Wanschura, M., Shevtsova, V., Kuhlmann, H.C., Rath, H.J.: Convective instability mechanisms in thermocapillary liquid bridges. Phys. Fluids **7**, 912–925 (1995)